3. THE PAYLOAD: DETECTORS, ELECTRONICS, AND STRUCTURE

Two different types of detectors were used for Hipparcos—the image dissector tube detector which sampled the modulated images of the stars as they crossed the main field of view, and the star mapper (photomultiplier) detectors, which sampled the entire field of the star mapper. The resulting signals provided the main sources of data analysed in the ground processing. There were two photomultiplier detectors for each star mapper channel, sampling the visual and blue wavelength ranges respectively. Mechanisms were used within the payload to protect the detectors as the fields of view swept across the illuminated Earth or Moon, to switch between the prime and redundant image dissector tube detectors (and introduce the corresponding internal star pattern assembly, used for geometrical calibration, into the field of view), to introduce the chromaticity calibration filter into the image dissector tube relay lens, and to adjust the focus position of the modulating grid. Each of the telescope's fields of view was protected by 'external' and 'internal' baffles, attenuating straylight from the Sun, Earth and Moon, and minimising the 'dead time' due to Earth and Moon occultations. Extremely high thermal and temporal stability of the relative positions of the optical components was also required.

3.1. Detectors

The function of both the main detection chain and the star mapper detection chain was the detection of the images of stars, which were modulated by the grid and focused by the relay optics, as described in Chapter 2. The photons detected were converted into electrical signals, and the processed signals were output according to a given protocol between the detection subsystem and the remote terminal unit.

The detection subsystem was located on the focal-plane assembly platform. It consisted of prime and redundant halves, each containing main and star mapper chains. As the power and switching of each section was independent, cross-strapping was provided, allowing either or both detection chains to be in operation in both halves of the subsystem. The star mapper detection chain was also responsible for the acquisition of data used for the Tycho experiment.

Main Detection Chain

The main detector assembly was an electro-optical and mechanical unit, whose function was to detect a light flux in a specific area and to convert this flux into an electrical signal. It contained the image dissector tube, the focus and deflection coils (including two-fold magnetic shielding), the high-voltage power supply (providing the required high voltages to the image dissector tube), the voltage divider network (providing the required intermediate high voltages to the individual dynodes of the image dissector tube), an isolation amplifier (providing the image dissector tube analogue output), and the pulse-amplifier and discriminator circuit (providing the image dissector tube pulse-counting output).

Under nominal operating conditions, only one of the two main detector assemblies was in operation, the other being available for redundancy reasons. The main detector assembly detected the light transmitted through the main grid from stellar images crossing the grid. The image dissector tube detected photons arriving at the photocathode in a small well-defined area, called the 'instantaneous field of view'. By appropriate control of currents through the deflection coils, this instantaneous field of view, of about 38 arcsec diameter, could be positioned to 'view' any location of the useful area of the photocathode. In this way, the detector was able to follow several stars on the main grid quasi-simultaneously, switching rapidly from one star image to another and detecting the photons from each star for a short period of time, defined by the star observing strategy.

The main detector assembly was designed to be used in both photon counting mode for faint stars and in analogue mode for bright stars. In photon counting mode, each photo-electron pulse is amplified, discriminated with an optimum threshold in order to improve the signal-to-noise ratio, and the output transmitted to a counter in the detection electronics box. In analogue mode, the photocathode current is amplified in the tube and the output current is directly converted into a digital word by means of a voltage-to-frequency converter in the main detector assembly. The output is transmitted to a counter in the detection electronics box.

The pulse counting channel counted the pulses at the anode of the image dissector tube caused by the photons which entered the instantaneous field of view. It consisted of two main parts: the part that brought the anode pulses into a shape suitable for a digital counting device; and a digital counter (the data compression circuit), which counted the resulting pulses. A block diagram of the pulse counting channel is shown in Figure 3.1.

The analogue channel (selected by telecommand) was designed to be used for the observations of the very brightest stars (brighter than about 1–2 mag), where the light input in the instantaneous field of view of the image dissector tube would be so high that a large number of pulses could no longer be recognised individually by the pulse counting channel. In order to avoid coupling problems with the pre-amplifier of the pulse counting channel, the current was measured on the last dynode of the tube.

A digital interface with the remote terminal unit provided data to the remote terminal unit and received memory load commands from it. The 16-bit memory load commands from this unit were converted into focus and deflection currents, or into high-voltage settings. Service signals (to clocks, power supplies, and test pulse generator) were also generated by the detection chain.

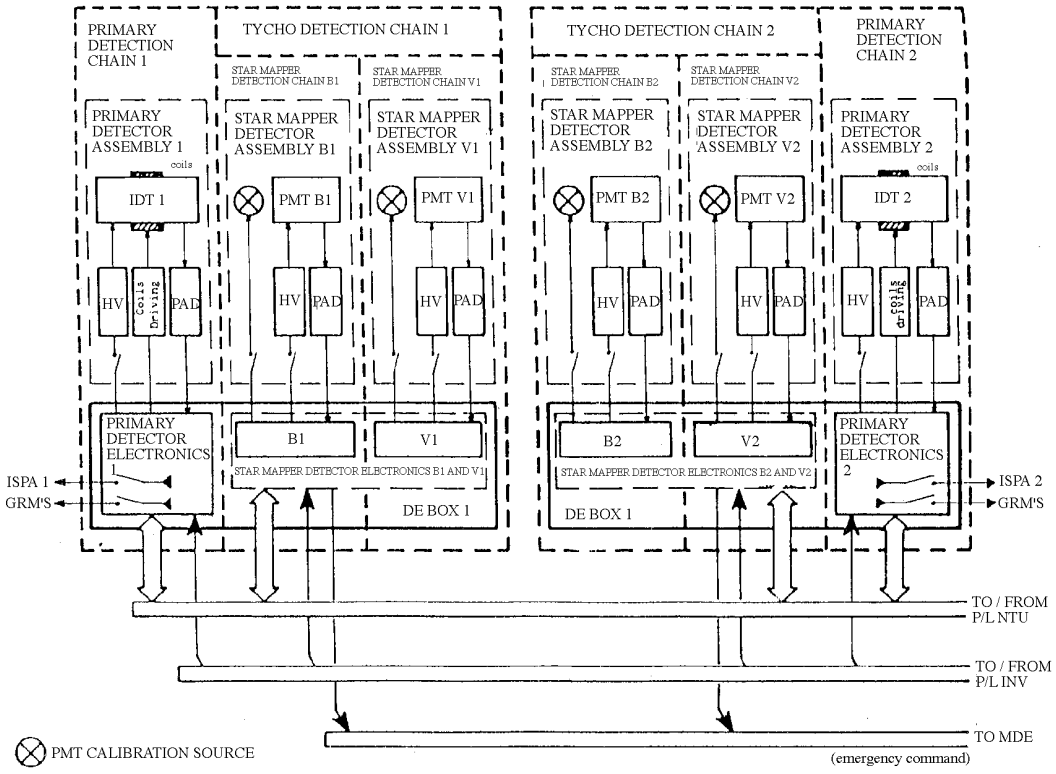

Figure 3.1. *Detection subsystem block diagram. The figure shows the schematic arrangement of the image dissector tube (IDT) and photomultiplier tube (PMT) detection chains, the latter used for the star mapper (Tycho) measurements. Each star mapper detection chain included a B_T and V_T channel, and each of the primary and star mapper detection chains was duplicated for redundancy reasons. (DE: detector electronics; HV: high voltage; ISPA: internal star pattern assembly; GRM: grid reference mark; P/L: payload; MDE: mechanism drive electronics.)*

The main detector assembly received its power from the detection electronics box and included its own high-voltage power supply, delivering the image section voltage, fixed at 400 V, and the multiplier section voltage, which could be adjusted by ±20 per cent around its nominal voltage of 1200 V by telecommand through the detection electronics box. The exact value of the high voltage was selected so as to have a nominal gain for the multiplier of 5×10^5.

For correct image dissector tube operation, the focus current had to be adjusted to obtain a good instantaneous field of view profile. The deflection currents of the image dissector tube were updated, during normal operations, at a frequency of 150 Hz (corresponding to 'slots' of the star observing strategy, as described in Chapter 8). These deflection currents defined the exact positioning of the instantaneous field of view at any instant.

Image dissector tube: The image dissector tube is a photomultiplier tube with a simple electromagnetic deflection system to sample one small part of its photocathode at a time. It had no memory to store an image, and so a strict sampling protocol was not required. The principle of operation is illustrated in Figure 3.2.

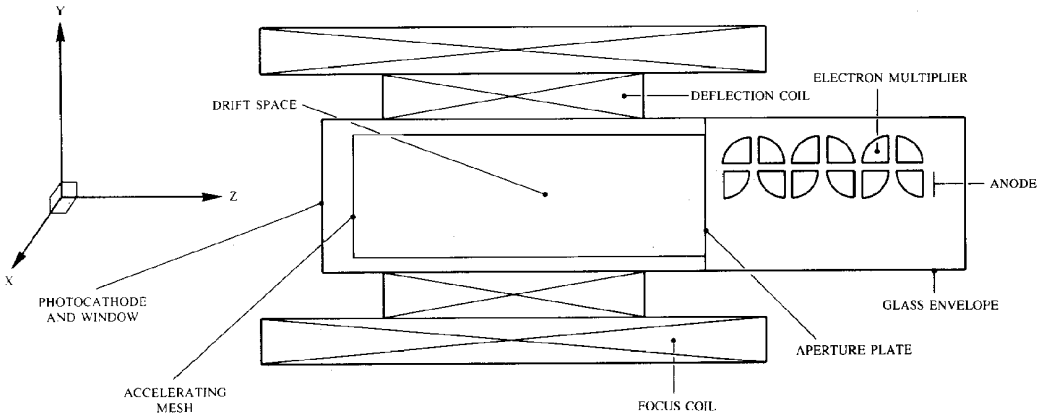

Figure 3.2. *Operating principle of the image dissector tube. Light reaches the photocathode from the left. The deflection coils ensure that light is detected from a small region of the photocathode, determined by the coil currents applied.*

The tube was constructed like a normal photomultiplier as far as the electron multiplier part was concerned. Between the photocathode and the first dynode, an electro-optical system was inserted for focusing and deflection. The electron multiplier and electro-optics were separated by an aperture plate with a dissecting aperture. In the case of Hipparcos, this aperture was circular with a diameter of 110 ± 2.5 μm (corresponding to about 38 arcsec on the sky).

The image dissector tube used for Hipparcos was a standard ITT (F4012 RP) tube without design modifications. The two-fold shielded focus and deflection coils were manufactured according to an existing design, with minor modifications to inner diameter and length of the assembly. The window was a plane-parallel (Dynasil 1000) fused silica plate carrying a semi-transparent S20 photocathode at the inner side of the tube. The photocathode was a thin light-sensitive layer which emitted electrons when photons were absorbed. The photocathode was deposited on a very thin transparent conducting layer, which compensated for the charge emitted by the photocathode.

The accelerating mesh was at a positive voltage with respect to the photocathode to extract the electrons from the photocathode area and to accelerate them in the direction of the drift space. A magnetic field was applied to the drift space by means of three coils (X-deflection, Y-deflection and focus). Emitted electrons followed orbits around the magnetic field lines and hit the aperture plane or passed through the aperture, depending on their points of origin on the photocathode.

Electrons passing through the aperture were collected by the first dynode, which produced secondary electrons with a certain efficiency. These electrons were collected by the second dynode and the process was repeated. At the end, all electrons produced were collected at the anode and the charge was amplified and processed further in the electrical system. The efficiency of the image dissector tube detector as a function of wavelength is given, as part of the overall payload transmission, in Table 2.2.

Star Mapper Detection Chain

The star mapper detector assembly was an electro-optical and mechanical unit, whose function was to detect a light flux and to convert this flux into an electrical signal. Four photomultipliers constituted the whole detection subsystem. In nominal operating conditions, two of the four star mapper detector assemblies were functioning, while the other two were available for redundancy reasons. In operation, the star mapper detector assemblies detected the light of stars that passed across the payload's star mapper grids. In each combination, the two photomultipliers were dedicated to a specific bandpass, with a wavelength centred at about 430 nm for the B_T photomultiplier chain, and at about 530 nm for the V_T photomultiplier chain.

Each star mapper detector assembly contained: a photomultiplier tube with shields against radiation and magnetic fields; high-voltage supply circuits (providing the required high voltage to the photomultiplier); a voltage divider chain (providing the required intermediate high voltages to the individual dynodes of the photomultiplier); a pulse-amplifier and discriminator circuit, for electrical processing of the electrical pulses produced in the photomultiplier, as a result of detection of photons at the photomultiplier photocathode; an anode-current monitor circuit, enabling the detection subsystem to generate an emergency command in case of over-exposure of the photomultiplier; and a light-emitting diode, providing optical test input to the photomultiplier.

Each detector assembly also had a mechanical structure, mechanical interfaces between the star mapper detector assembly and the focal-plane assembly, and electrical interfaces. The detection chain also generated service signals (to clocks, power supplies, and test pulse generator).

Photomultiplier tube: The photomultiplier tube used for Hipparcos was a special version of the Thorn-EMI 9924 B tube. The anode was modified as a result of extensive vibration tests performed by the manufacturer. The window was made as thin as possible, to reduce Cerenkov radiation caused by absorbed high-energy electrons. To increase the sensitivity, the window surface was vapour-blasted.

The photomultiplier had a 30 mm outer tube dimension, with a 23 mm effective cathode diameter. The photocathode had a bi-alkali spectral sensitivity. Photo-electrons, produced in the photocathode by incident photons, were amplified by means of 11 successive box-and-grid dynodes creating, on the photomultiplier anode, a charge pulse of $5 - 10 \times 10^6$ electrons per detected photon. The efficiency of the photomultiplier tube detectors as a function of wavelength is given, as part of the overall payload transmission, in Tables 2.3 and 2.4 for the B_T and V_T channels, respectively.

Detection Electronics Box and Signal Coding

The detection electronics box was an electronic unit whose main functions were: to interface with the remote terminal unit, inverter, and mechanism drive electronics; to interface with the main detector assembly and star mapper detector assemblies; to generate power supplies from the AC power; and to generate digital data from the star mapper detector assemblies and main detector assembly output.

Since the detection electronics box was the only interface for telemetry and telecommand, it received on/off commands for proper configuration of the detection subsystem, one 16-bit memory load command for the main detection chain (used for high-voltage setting, focus current, deflection current, and test generation operation), and one memory load command for the star mapper detection chain and test generation operation (this command was used for high-voltage setting of the B_T and V_T photomultipliers).

The detection electronics box was the interface for the transmission of scientific data. For each primary detection chain, sampled at 1200 Hz, the scientific data consisted of one serial digital 8-bit channel corresponding to the compressed data word in pulse-counting mode, and to the analogue-to-digital converter word in analogue mode (the pulse-counting or analogue-to-digital word was sent to the ground according to the status of an appropriate bit in the programme star file uplinked to the satellite).

For each star mapper detection chain, the scientific data, sampled at 600 Hz, consisted of one serial digital 16-bit word resulting from the concatenation of the two compressed 8-bit data words coming from the two star mapper detector chains—the most significant bits containing the V_T data, and the least significant bits containing the B_T data.

In photon counting mode, the 8-bit scientific data (for both the primary detection chain and the star mapper detection chain) represented the number of counts corresponding to the sampling period (1200 Hz for the primary detection chain, and 600 Hz for the star mapper chain), applying a 'semi-logarithmic' data compression. The maximum count rate that could be coded in pulse counting mode using this compression law was 8159 counts per sample, corresponding to a maximum flux for the image dissector tube data of 9 790 800 counts per second, and 4 895 400 counts per second for the star mapper data.

In this compression, the 8-bit word was the concatenation of a 5-bit mantissa, M, and a 3-bit exponent, E. The determination of E and M for counts, N, in the range $0 \leq N \leq 8159$ proceeded as follows: first the exponent E was determined such that $2^E \leq 1 + N/32 < 2^{E+1}$, then M was taken to be the integer part of $(N + 32)/2^E - 32$. Note that counts up to $N = 31$ were coded without loss of information ($E = 0$, $M = N$); this condition applied to all stars fainter than $B = 7 - 8$ mag.

Assuming image dissector tube count rates of between 2000–4000 counts per second for a star of $B = 9$ mag, depending on star colour, this implied that the analogue mode would be required for the observations of stars brighter than $B = 1 - 2$ mag. Similar considerations for the star mapper implied that the photon-counting channel would saturate for stars brighter than about $B = 2 - 3$ mag. In the case of the star mapper channel, no analogue mode was available, and stars brighter than the saturation threshold were not expected to yield valid data; this was not considered to be a limitation in the design, since the function of the star mapper was primarily one of real-time attitude determination, and the threshold limit for the use of stars as attitude 'reference' in the real-time attitude determination algorithm on-board was fainter than this saturation limit, actually about $B = 4 - 5$ mag, due to the range over which the reference star magnitude could be coded on board.

In practice, the analogue mode for the image dissector tube was not used, the photon counting mode being satisfactory even for the very brightest stars, while the star mapper observations were similarly only marginally affected for the brightest stars.

3.2. Payload Electronics and Mechanisms

The Payload Service Electronics

Mechanism drive electronics: The mechanism drive electronics unit supplied the motors for the mechanisms within the payload with suitable pulses. The programming was transferred via memory load telecommands from the payload remote terminal unit. The mechanism drive electronics unit also provided conditioned status information about the mechanisms to the remote terminal unit. Three different interface types were foreseen to drive the stepper motors, electromagnets, and torque motors.

The mechanism drive electronics unit contained two completely stand-by redundant mechanism control electronics, inclusive of AC/DC converters. Each one was able to drive and monitor all mechanisms. Mechanisms were driven by power pulses delivered by one of the two mechanism drive electronics sections. Both redundant chains were controlled and monitored by the payload remote terminal unit.

Thermal control electronics: The thermal control electronics provided the transformation of resistance values from housekeeping and temperature control thermistors into analogue voltages, the acquisition and processing of six memory load commands (containing control information for the heater DC-voltage levels and allocation of individual DC-voltage levels from the primary DC bus to payload heaters), and the generation of secondary DC-power for internal supply of the thermal control electronics powered by cold-redundant AC-buses.

The thermal control electronics included two redundant sections, with the exception of the housekeeping thermistor-conditioning circuits. These circuits were supplied with secondary power from both sets of thermal control electronics, which were dedicated to the 24 thermally controlled areas, nominal and redundant heaters, and thermistors. Both chains were controlled by the payload remote terminal unit.

Mechanisms

The following mechanisms were contained within the payload:

(1) the refocusing mechanism, which interfaced with the grid package and associated mirror necessary to fold the main beam. This mechanism allowed the focusing of the grid position with respect to telescope focal surface;

(2) the switching mirror mechanism, which provided the mechanical support to the switching prism. It allowed the optical beam to be switched to one of the two redundant main detectors;

(3) the two chromaticity mechanisms, one per image dissector tube channel; each was equipped with a chromaticity filter and a wide-band filter. Switching from the wide-band filter, which was used in normal operation, to the chromaticity filter allowed in-orbit calibration of the payload chromaticity;

(4) the four shutter mechanisms, which protected the detectors from light overload damage.

Refocusing mechanism: The main function of this mechanism was to allow the grid unit to be refocused during the mission to compensate for factors having long-term effects on the focus position, in particular moisture release and optical surface deformation as a result of radiation damage. The mechanism was split into four separate parts (Figure 3.3): the linear actuator, the linkage, the parallel movement element, and the mechanism frame.

The linear actuator comprised a stepper motor, a two-stage gear box, and some monitoring devices. The motor was activated via the mechanism drive electronics and drove the refocusing mechanism spindle. This spindle movement was transformed into a parallel motion of the grid, via the linkage, and the grid unit was moved along the optical beam axis direction. One cycle activation corresponded to four elementary motor steps, and induced a spindle displacement of 46 μm, which resulted in a grid movement of 1.2 μm. The total grid movement amplitude was $\pm$1.2 mm with respect to the mid-position.

The position of the spindle of the linear actuator was monitored by a linear potentiometer (a device capable of converting the movement along a straight line into a resistance change proportional to the displacement). The resistance range was about 1330 – 3670 Ω. The linear potentiometer did not give a very accurate indication of the refocusing mechanism's position (the accuracy was about 50 μm), and was used only as a real-time check that the refocusing mechanism was working nominally. A special coupling was used which freed at a force higher than about 20 N if the potentiometer jammed.

Each end of the linear actuator spindle stroke was monitored by two reed-switches, one being for redundancy reasons. The linkage was used to convert the displacement of the linear actuator into a reduced displacement of the grid barrel. The linkage was built from three spring blades. The two main blades were bolted to the mechanism frame and to the grid barrel, respectively, with zero-tolerance fixtures to ensure a high stability. The blades were fixed to each other at their other ends in a connecting block. From this block, a thinner spring blade went to the linear actuator. Parasitic rotation of the linkage-blades was prevented by two bearing wheels guiding the spindle of the actuator.

This linkage, made of titanium alloy, led to a reduction in the displacement, which varied from 1 : 4.08 to 1 : 4.76 in extreme positions. All connections between the parts of the linkage were made by electron beam welding performed in high vacuum. The parallel movement was required to shift the grid along its stroke without parasitic movements. To that extent, the guidance of the grid barrel was designed with circular springs to ensure low parasitic rotations around the optical beam axis. The parallel movement element was divided into the grid support unit and the folding mirror. The grid support unit consisted of the mounting for the grid mount and the barrel, which connected the membrane supports and the folding mirror system. Openings for the optical beams toward the main detector assembly and star mapper detector assembly were made in this barrel.

The attachment for the grid mount was on one side of a circular invar tube with two rigid lugs to connect to one of the springs, and four smaller lugs to fix the grid mount and the baffle unit. All fixtures were with zero tolerance. In this way, a stable base was created which allowed mounting and dismounting of the grid assembly with a good reproducibility. On the other side of the tube, four rigid lugs were available for connecting both the half membranes. There were also provisions for mounting the folding mirror and connection to the linkage.

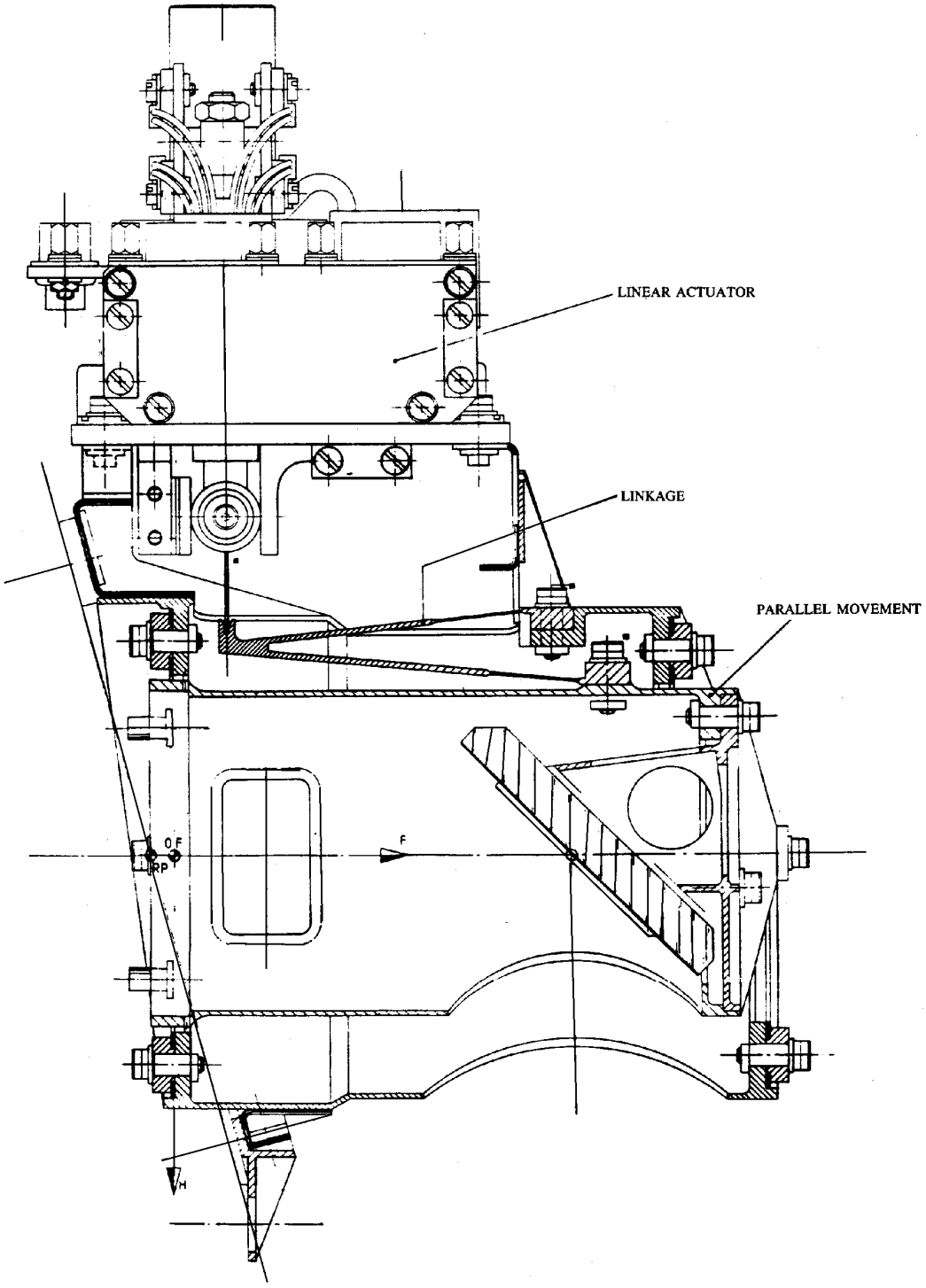

Figure 3.3. *General layout of the refocusing mechanism. The movement of the linear actuator in a vertical direction resulted in a much smaller movement of the refecting mirror, at the lower right, in a horizontal direction. The movement of the grid per refocussing step was 1.2 μm.*

The folding mirror was located at the back side of the grid barrel tube. This mirror, having an angle of 45° to the optical beam, deflected the main light beam towards the switching mirror and the main detector assembly packages. It was made of zerodur and was bonded in its mount, which was machined with sufficiently tight tolerances for there to be no need for adjustment. This mounting could be easily removed and re-installed with sufficient reproducibility, as a result of the zero-tolerance fixings.

The mechanism frame was the main structure to which the different assemblies were fixed: the parallel movement element with grid unit and baffle unit; the linear actuator; and the linkage. This frame was mounted onto the focal-plane assembly platform, using a device capable of adjusting the complete mechanism in three degrees of freedom to avoid the effects of shift and rotation during launch.

Flip-flop mechanisms: The basic function of each mechanism was to provide a two-position capability for the optical elements (filters and mirror) and the shutters. The principal differences between the types of mechanism were the rotation angle of the elements (45° for shutters and filters, and 90° for the switching mirror), the mass inertia and geometry of the different elements, and the accuracy and stability requirements for the different elements. The following operational modes were provided for each mechanism:

(i) normal mode, from rest to working position: on telecommand, the torque motor drove the element into its working position while torquing the spiral torsion spring. When the motor was switched off, the position was maintained by the attractive force between a permanent magnet fixed on the housing bracket and a soft iron core fixed to a paddle;

(ii) normal mode, from working to rest position: on telecommand, the torque motor drove the element back to its rest position. When the motor was switched off, the rest position was maintained by the rest torque of the spiral torsion spring;

(iii) back-up: the fail-safe device that provided partial drive redundancy consisted of the above-mentioned spiral torsion spring and an electromagnet mounted on the housing bracket. If a failure occurred in the nominal driving branch when the mechanism was in working position, the electromagnet could be activated. It produced a repulsive force, which compensated for the attractive force between the permanent magnet and associated soft iron core, and the spiral torsion spring drove the optical element back to its rest position.

The design was based on identical mechanisms for the main detector assembly and star mapper detector assembly shutters, and for the main detector assembly chromaticity filter. As far as the switching mirror was concerned, the design was adapted to more stringent accuracy and stability requirements.

Each mechanism consisted of a bearing box with an electrical torque motor as prime mover and a rotating shaft which carried the optical element. The mechanism housing was made of aluminium. The two mechanical end stops were located at the front of the mechanism in order to minimise the offset and the corresponding relative distortions between the moving element and its mechanical end stops.

The two end positions were maintained without power on the motor by means of the rest torque of the torsion spring in one position, and, in the other position, by the attractive force between a soft iron core fixed on the flip-flop disc and a permanent magnet fixed on

the mechanism bracket. The two ends of travel were monitored by means of reed end-switches mounted on the housing. The permanent magnet needed for activation of the reed switches was mounted on the flip-flop disc. A damping system was implemented on the flip-flop disc to reduce the rebounds generated in the mechanical end stops.

The mechanism bracket was made of invar to minimise the thermal load interaction between the mechanism and the focal-plane assembly. The aluminium housing was mounted on the bracket by means of three fixing points. A rigid fixing point was located at the front of the mechanism, and two flexible fixing points were located at the rear of the mechanism. The purpose of the two flexible fixings was to reduce the internal loads generated at this interface by the different expansions of the housing and the bracket under the given thermal environment.

Adjustment capabilities in the x, y, and z directions were achieved by means of shims. For x-direction adjustment, the shim was located between the flip-flop disc and the optical hardware; for the y-direction, on the fixing points between housing and fixing bracket; and for the z-direction, at the interface between the mechanism and the focal-plane assembly. The positioning accuracy caused by the x, y, and z adjustment operations was given by the shim manufacturing tolerances. Taking into account these tolerances the positioning accuracies of the flip-flop mechanisms were found to be within the specified initial positioning accuracy range. The interface to the electrical harness was provided by means of a 15-pin connector fixed to the housing.

3.3. Baffles

The 'External' Baffles

Each of the two baffles was divided into three major constituents: the support structure, the baffle tube, and the front aperture assembly.

The support structure was formed by six struts, four attachments to the spacecraft upper platform, and one adjustment device on each strut. It supported the other components and provided for ground alignment of the baffle optical axis. The struts, shown in Figure 3.4, were carbon-fibre reinforced plastic tubes of diameters 30 and 40 mm, with a wall thickness of 1.2 mm. They had titanium fittings at each end. The attachments were aluminium milled parts, screwed to the spacecraft upper platform attachment points. On them were fixed the lower adjustment devices. The lower adjustment device was formed by half spheres, spherical washers, and nuts. When the nuts were loose, any change in length induced by turning the nut moved the baffle as a rigid body, without introducing any load because of the isostatic function of a six-bar system. When all nuts were tightened, the struts were fixed in length and angular position.

The main optical requirement for the baffle tube was that all light from outside a given Earth angle envelope had to be intercepted by a set of fins. In addition, it supported the front aperture assembly. It was formed by nine segments—two of them were structural with 2 mm wall thickness, while the others were mainly optical with 0.52 mm wall thickness.

For stability reasons, there was no mechanical contact between the baffles and the payload structure. A 'labyrinth' system was provided by means of a carbon-fibre reinforced

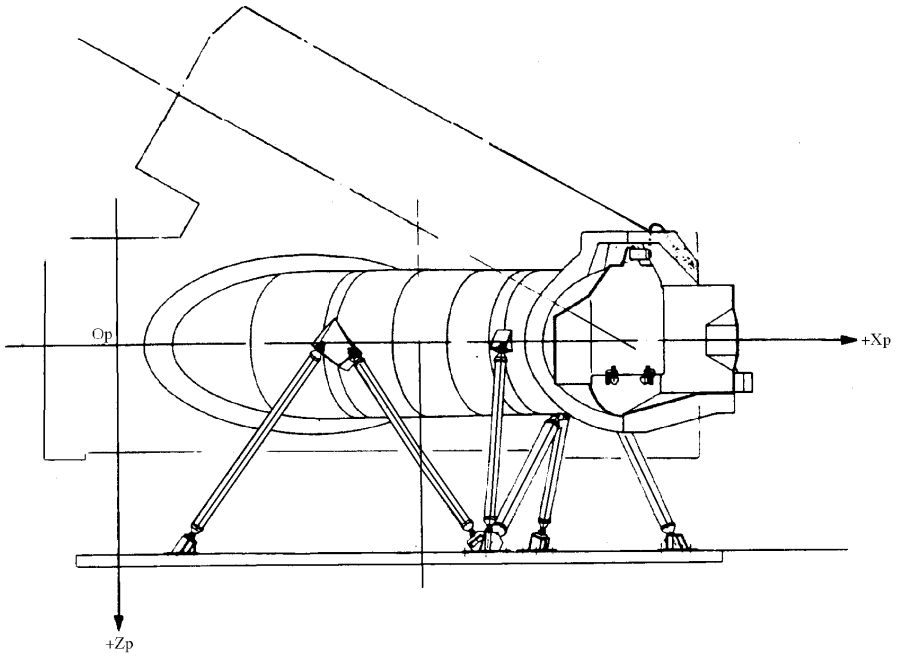

Figure 3.4. *The baffle assemblies. Light entered from the right of the figure. Internal 'labyrinths' suppressed the scattered light. The baffle assemblies were supported by struts to the spacecraft platform (below), mechanically decoupling them from the payload.*

plastic ring bonded on the baffle tube and the associated carbon-fibre reinforced plastic ring bonded on the payload structure. Four external brackets with aluminium reinforcements were bonded to the tube, onto which the upper adjustment devices were fixed.

In the front plate assembly, the front plate aperture defined the design beam envelope and the Earth angle envelope. The fixed screen and the cover in open configuration prevented any direct sunlight from reaching the front plate aperture. Moreover, the multi-layer insulation frame provided a flat mounting area for the shade structure thermal insulation. This assembly was formed by the front-plate fixed screen, the cover, hinges, the closing latch, the labyrinth, and the multi-layer insulation frame.

The front-plate fixed screen was a carbon-fibre reinforced plastic sandwich, fixed to the tube, on which the front plate aperture was machined. The hinges and the corresponding labyrinth and closing latch were fixed on the front plate. The cover was a carbon-fibre reinforced plastic sandwich panel connected to the front plate through the hinges and the closing latch in closed configuration. The other part of the labyrinth was fixed to it. There were two hinges in each baffle, so the system was redundant in driving torque, locking and monitoring.

During ground operations, and also throughout launch and the early operations, the baffles were closed by the covers, in order to protect the optics against contamination. When closed, the covers ensured the required telescope venting during launch and during transport by aircraft, through the labyrinth and venting holes. The covers were deployed in orbit by means of a pyrotechnic device. When opened, the cover prevented sunlight entrance into the baffle.

The 'Internal' Baffles

A set of internal baffles was connected to the main structure. Their prime function was to ensure separation of the half-pupil beams and of telescope inner enclosures, and consequently help to meet the light-tightness and straylight requirements. These baffles comprised:

(1) the straylight pupil baffle, consisting of carbon-fibre reinforced plastic plates (thickness 0.7 mm) assembled by means of bonded carbon-fibre reinforced plastic corner profiles. This baffle was located approximately half way between the beam combiner and the folding mirror, and was connected to the $+Z$ panel of the main structure and to the enclosure separator baffle by means of anchor floating nuts and screws;

(2) the enclosure separator baffle, consisting of a carbon-fibre reinforced plastic plate (thickness 0.7 mm) and parallel carbon-fibre reinforced plastic stiffeners (thickness 1.44 mm) bonded and riveted. This baffle was connected to the stiffener of the lateral panels by means of the two hard points and ten flexible blocks, cutting the enclosure into two parts: the beam combiner mirror plus folding mirror part, and the spherical mirror plus folding mirror part;

(3) the beam separator baffles, consisting of carbon-fibre reinforced plastic plate (thickness 0.7 mm) with a beam-shaped hole. These baffles were located around the two beam entrance apertures and were connected to lateral panels of the main structure by means of screws and floating anchor nuts;

(4) the pupil baffle, consisting of a box made from aluminium (type AG5) sheets of 0.3 mm thickness and black painted. Surrounding the beam combiner, it was connected to the barrel by means of blades;

(5) the grid baffle, attached to the grid assembly and described in Chapter 2;

(6) Cerenkov shielding: the external sides of the focal-plane assembly cover were equipped with shielding to protect the optics against Cerenkov radiation. The shielding, with a total weight of 2 kg, was made of aluminium sheets bonded on the external skin of the focal-plane assembly cover.

Straylight Performances

The main function of the baffles was to attenuate parasitic light coming from the Sun, the Earth and the Moon which would otherwise fall on the detectors. Straylight originating from the Sun was specified to be less than the average sky background (using a background figure of $B = 22.5$ mag arcsec^{-2} and a colour index of $B - V = 0.7$ mag), and straylight coming from the Earth or the Moon was specified to be less than ten times the background (defined to be the 'interruption limit'), when these bodies lay outside a rectangle of $\pm 24°$ (in the scan direction) by $\pm 13\overset{\circ}{.}5$ (in the transverse direction), centred on the optical axis.

The straylight performances of the payload, which also depended on mirror scattering, were measured before launch in a dedicated test using a light source representing the

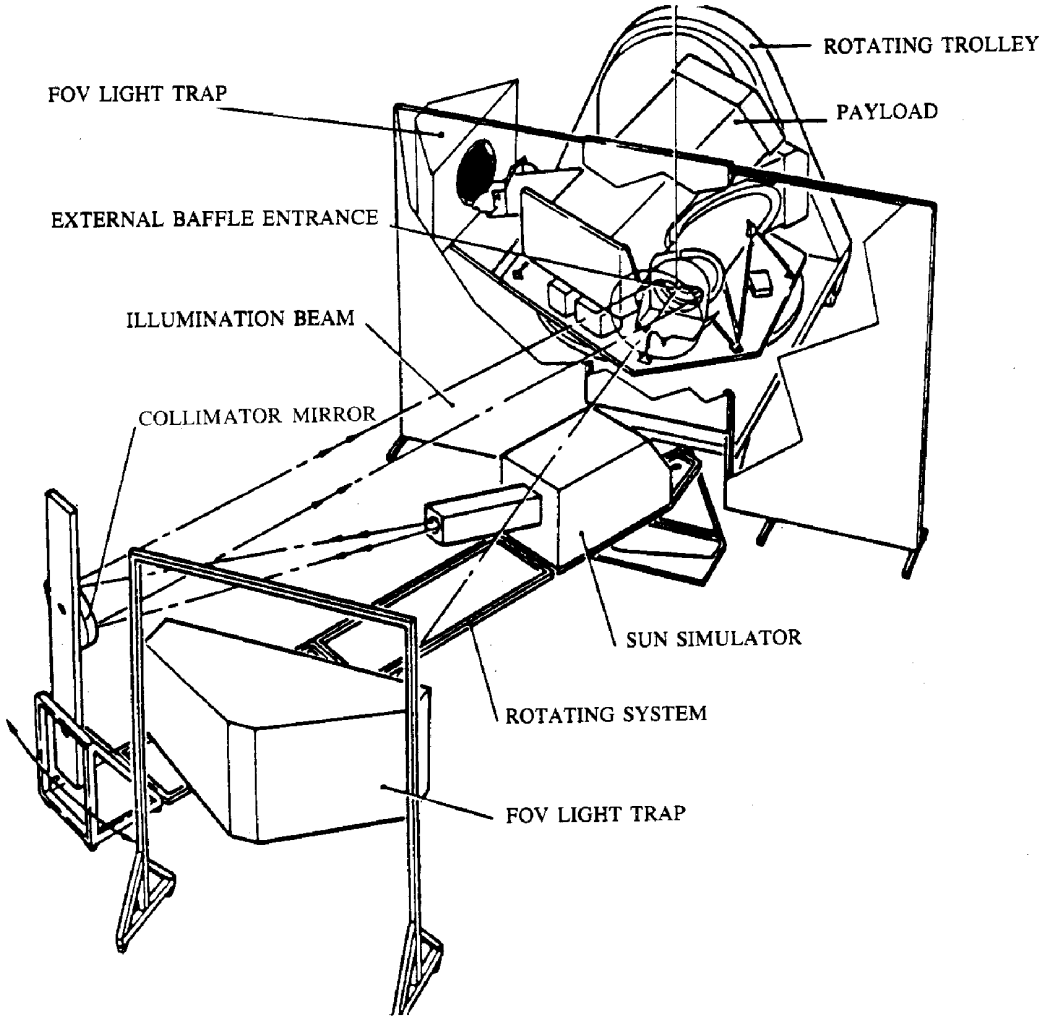

Figure 3.5. *Straylight test configuration. The rotating system moved the light source to different angles with respect to the viewing direction, leading to the production of the straylight attenuation curves shown in Figure 3.6. The light trap was directly in front of the entrance aperture, preventing other light from entering the payload.*

Moon directed onto the baffle aperture. The simulator was rotated around the baffle entrance along each of eight directions with respect to the scan axis, to provide representative positions of the illuminating source (see Figure 3.5). Measurements were corrected to account for the scattering of incident light due to the presence of air, and straylight performances for the Earth were computed from the measurements. Attenuation of the sun straylight was evaluated by simulating worst cases of sun aspect angle using the same simulator.

Measurements of the detected straylight intensity at a given position in the field of view, and of the incident light intensity on the baffle aperture, provided the data with which to determine the 'attenuation' in that direction, defined as the ratio of the equivalent straylight on the baffle aperture to the incident irradiance in the same direction (attenuations are therefore expressed in sr^{-1}). Figure 3.6 shows an example of an attenuation curve applicable to the case of the full Earth moving in the scan direction and crossing

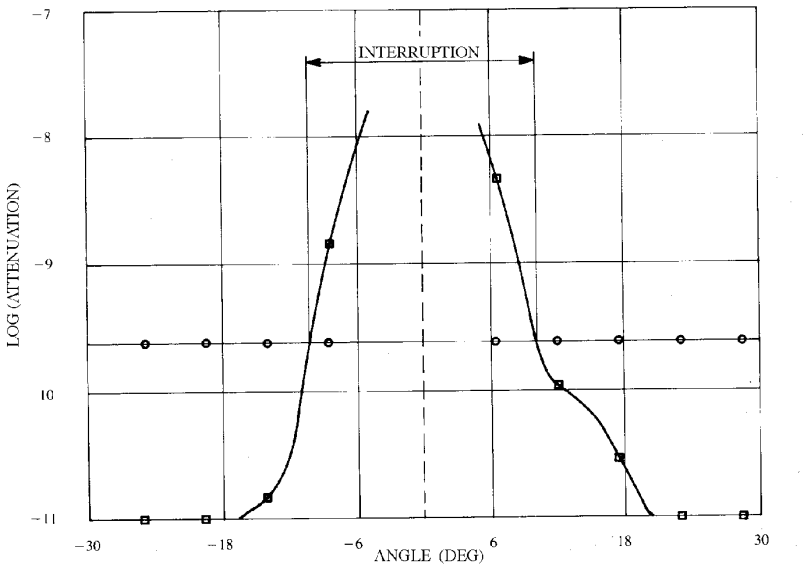

Figure 3.6. *Straylight attenuation curves. The squares show the measured attenuation, the circles show the accepted straylight 'interruption limit' of ten times the average sky background.*

the baffle axis. In this example, the straylight level is higher than ten times that of the sky background over a region 20°.3 wide, well within the specified 24°.

Straylight attenuation in the scan direction mainly influenced the duration of the interruptions of the observations. The corresponding dead time, averaged over the mission, was estimated to be about 5 per cent for a geostationary orbit. The number of interrupted scans, determined by the attenuation in the transverse direction, was predicted to be around 33 per cent, again for the nominal geostationary orbit.

3.4. Payload Structure

The payload structure subsystem provided the mechanical support for all other payload items—the telescope mirrors (the beam combiner, the folding mirror and the spherical mirror), the focal plane assembly platform (comprising the refocusing mechanism, the grid assembly, the relay optics, the detection subsystem, and the mechanisms), the thermal control hardware, and the harness.

The telescope structure was designed to maintain the accurate relative positioning of all optical surfaces, including the three telescope mirrors, and the elements of the focal plane assembly. Consequently, the structure had to be extremely stable over the entire period, from final alignment on ground until the end of mission in orbit. Such stringent alignment requirements had to be maintained in the face of the launch environment; thermal environment variation; mechanical interfaces with the satellite, focal plane assembly units and harness; variation of humidity; and the effect of gravity release.

The structure had to induce very low bending moments on the mirrors, to minimise optical surface deformations. Isostatic connection to the spacecraft was required; and the structure furthermore had to provide light tightness, maintain cleanliness, ensure

the easy implementation of thermal hardware and a maximum mechanical decoupling between structural and thermal hardware, and facilitate the integration.

The overall telescope structure was split into a primary structure (consisting of the main structure, the focal plane assembly platform and the mirror mounts), and a secondary structure (consisting of the internal baffles, the beam combiner and spherical mirror covers and focal-plane assembly cover, and the heater mat carriers). The following section provides a design description of the various sub-assemblies of the telescope structure.

Main Structure

The main structure was partially dismountable, with a door in the upper panel, providing easy integration without complex assembly tools, and access into the telescope structure during integration and test activities.

The overall optical layout, and the mass, stiffness, and stability requirements called for a box-type structure made with carbon-fibre reinforced plastic skin panels and stiffeners or carbon-fibre reinforced plastic shear panels linked by corner profiles and folded edges (see Figure 3.7).

For the five enclosure panels, a carbon-fibre reinforced plastic product was used, consisting of 12-ply multi-layers (using ultra-high-modulus GY 70 carbon fibre, which gave a very low coefficient of thermal expansion (of order 10^{-7} K^{-1}), with a high Young's modulus (about 10^5 N mm^{-2})). Where local reinforcements were needed, a number of carbon-fibre reinforced plastic face sheets were added (with the same lay-up) and bonded together.

The junction between the panels was achieved either by folded edges or by corner profiles bonded and riveted on panels, except for the door of the upper panel, which was dismountable and assembled with floating anchor nuts and expandable pins to avoid any relative movement of the carbon-fibre reinforced plastic parts.

The mounting hard points were bonded on carbon-fibre reinforced plastic skins and riveted together. Invar was used for the barrel interface because of its low coefficient of thermal expansion (2×10^{-6} K^{-1}), which was required for thermal stability and low bonding stresses in the expected thermal environment. Titanium was used for the interface structure for lightness. Fittings were designed to have a good torsion and bending stiffness, to avoid micro deformation due to local low stiffness and areas of stress concentration. The payload was bonded on the centreline of a carbon-fibre reinforced plastic supporting framework, which had a good bending and torsional stiffness.

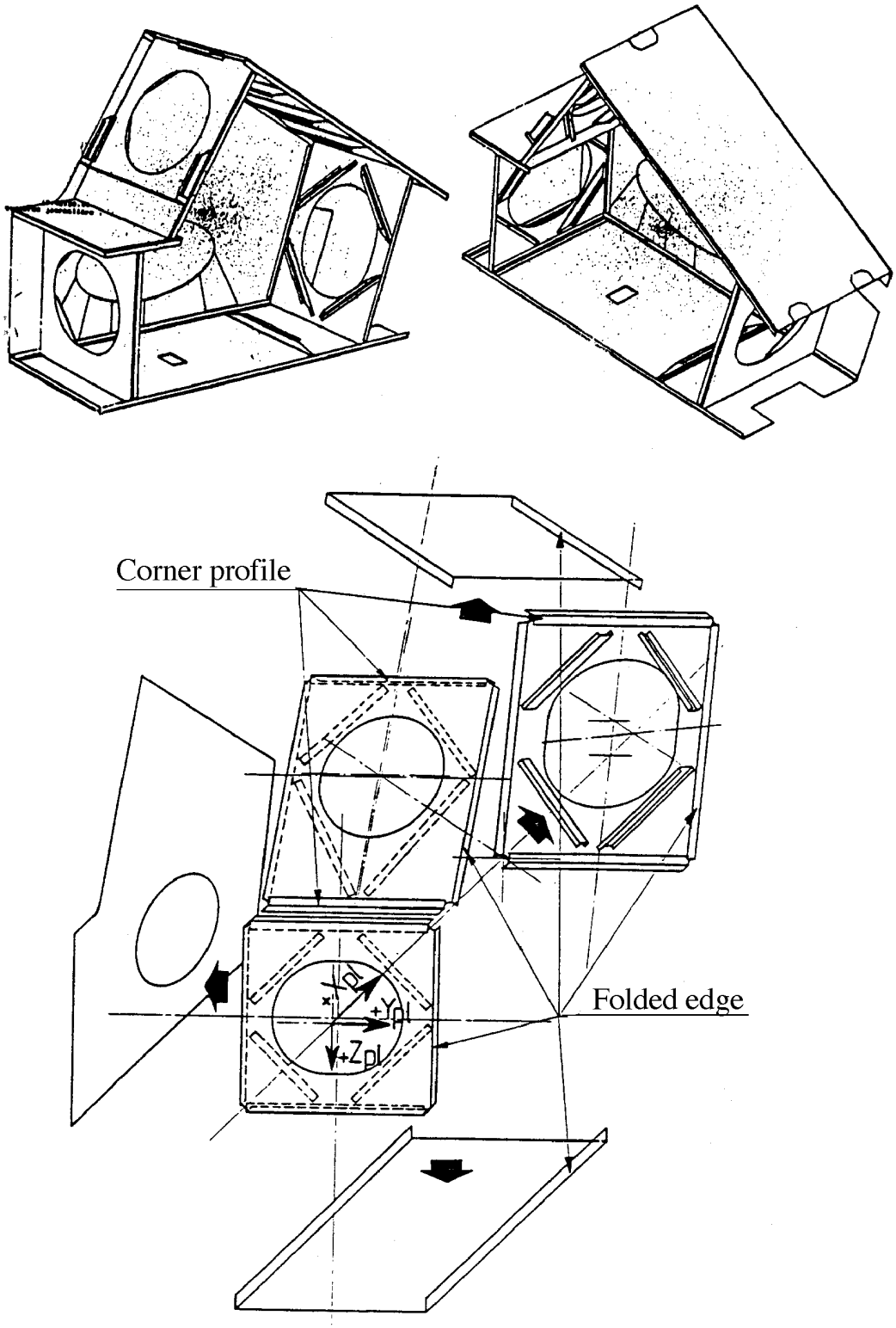

Figure 3.7. *The main structure. The structure was based around carbon-fibre reinforced panels, which were bolted together, with additional stiffeners in the areas of the aperture openings.*

Mirror Mounts

This sub-assembly consisted of a carbon-fibre reinforced plastic frame 'barrel' linked to the main structure by means of three rigid fixings, and three flexural pivot blade systems joining the mirror to the barrel.

The frame barrels were sandwich platforms with aluminium (AG5) honeycomb and carbon-fibre reinforced plastic skins. They had a hole in their centres, the external shapes being either triangular for the beam combiner and the spherical mirror, or quasi-circular for the folding mirror. In areas where loads were concentrated, there were carbon-fibre reinforced plastic thick plate reinforcements bonded on the sandwich. The different fixation hard points (with flexural pivot blade system and with telescope structure) were fixed with invar inserts, which were bonded and riveted on carbon-fibre reinforced plastic. The adjustment device for mirror and barrel alignment had six degrees of freedom, the adjustment being carried out by means of adjusting shims. Expandable pins were added to avoid relative component movements, in order to meet the long-term stability requirements.

A typical mirror mount set comprised three flexural assemblies, fixed symetrically at the periphery of the mirror. Each of the three assemblies was composed of a titanium cruciform section and an invar blade section. The cruciform section, attached to the mirror by 12 screws through an invar pad bonded on the mirror, behaved as a hinge around the radial direction and minimised the radial torque induced by barrel deformations. The solution of invar pads bonded to the mirror was selected because it was considered preferable to have separate thin pieces bonded to a mirror, instead of big pivot blades, during mirror polishing.

To improve long-term stability performance, positive fixings were implemented between pivots and pads by means of two expandable pins per pivot. The invar blade section was rigid around the axes tangential to the mirror edge. To minimise moments introduced during integration, the blade and the cruciform sections were assembled with spherical surfaces which had to be blocked, after alignment of the mirror, by means of a screw.

Focal-Plane Assembly Platform

This platform was designed to support 39 kg of equipment, and had to ensure a first frequency higher than 100 Hz. It was made of carbon-fibre reinforced plastic sandwich panel rigidly connected by eight points to the edges of panels of the main structure. Mounting of equipment and mechanisms onto the platform was achieved through some 110 bonded inserts equipped with studs.

The basic panel was made from aluminium honeycomb with carbon-fibre reinforced plastic skin, consisting of 18 ply multi-layers ultra-high-modulus GY 70 carbon fibre, which gave a very low coefficient of thermal expansion with a high Young's modulus. The focal-plane assembly platform's integration on the main structure required four degrees of freedom for alignment, where tilt adjustment was performed by means of adjusting shims. To avoid micro displacement of the focal-plane assembly platform with respect to the telescope, four expandable pins were added on four fittings. These fixing techniques provided a reproducibility that allowed mounting and dismounting activities to be undertaken without loss of the correct positioning.

Cerenkov Shielding

Some of the optical elements, such as the grid and the relay optics, generated photons (Cerenkov effect) and were expected to degrade in transmission ('darkening') as a result of irradiation by high-energy electrons in geostationary orbit. Such optical elements were protected by the so-called 'Cerenkov shielding'. A total of about 12 kg of protective material was placed around the relay optics and on the shade structure, complementing inherent shielding provided by the structure and the equipment surrounding the sensitive optical elements.